Measurement of detection efficiency using Pb-scintillating fiber sampling KLOE calorimeter for neutrons between 22 and 174 MeV

M.Anelli[a], G.Battistoni[b], S.Bertolucci[a], C.Bini[c], P.Branchini[d], C.Curceanu[a], G.De Zorzi[c], A.Di Domenico[c], B.Di Micco[d], A.Ferrari[e], S.Fiore, P.Gauzzi[c], S.Giovannella[a], F.Happacher[a], M.Iliescu[a,f], M.Martini[a,h], S.Miscetti[a], F.Nguyen[d], A.Passeri[d], A.Prokofiev[g], P.Sala[b], B.Sciascia[a,1], F.Sirghi[a]

Institutions:

(a) Laboratori Nazionali di Frascati, INFN, Italy,

(b) Sezione INFN di Milano, Italy,

(c) Università degli Studi "La Sapienza" e Sezione INFN di Roma, Italy,

(d) Università degli Studi "Roma Tre" e Sezione INFN di Roma Tre, Italy,

(e) Fondazione CNAO, Milano, Italy,

(f) IFIN-HH, Bucharest, Romania,

(g) The Svedberg Laboratory, Uppsala University, Sweden.

(h) Dipartimento di Energetica dell'Universitá "La Sapienza",Roma, Italy.

(1) Corresponding author: barbara.sciascia@lnf.infn.it

***Abstract*—We exposed a prototype of the high-sampling lead-scintillating fiber KLOE calorimeter to neutron beam of 21, 46, and 174 MeV, provided by the The Svedberg Laboratory (TSL), Uppsala, to study its neutron detection efficiency. This has been found larger than what what expected considering the scintillator thickness of the KLOE prototype only. We checked the reliability of our method, measuring also the neutron detection efficiency of a 5 cm thick NE110 scintillator. Our results prove the existence of a contribution from passive material to neutron detection efficiency, in a high-sampling calorimeter configuration. The origin of the efficiency enhancement has been studied using the FLUKA Monte Carlo code. We present the TSL beam test results and the reasons for such enhancement, which allows to develop compact, inexpensive, fast, and highly efficient neutron counters.**

***Index Terms*—calorimeter, neutron detection efficiency, scintillating fibers**

I. Introduction

Detection of neutrons with energies from a few to hundreds MeV is usually performed with organic scintillators. The high concentration of hydrogen atoms provides a proton target and the elastic scattering of neutrons produces recoil protons which produce a visible response. Typical efficiency is of the order of 1 % per cm of scintillator thickness [1]. On the other hand the extended range rem counters used in radiation protection [2], [3] are based on the idea of adding one layer of a medium-high Z material to the organic scintillator. This enhances the neutron response through inelastic processes that result in an abundant production of secondary neutrons.

The KLOE calorimeter [4] is a high sampling lead scintillating fiber calorimeter. Energy and time resolutions are $\sigma_E/E = 5.7\%/\sqrt{E(\mathrm{GeV})}$ and $\sigma_t = 57\ \mathrm{ps}/\sqrt{E\ (\mathrm{GeV})} \oplus 100\ \mathrm{ps}$. The calorimeter was primarily designed to detect photons, the detection efficiency is $\sim 90\%$ at $E = 20$ MeV and reaches 100% above 70 MeV.

A measurement [5] performed at KLOE using charged kaon interactions in the apparatus walls showed high efficiency for neutron of about 20 MeV of the KLOE calorimeter. The average efficiency measured was between three and four times higher than the one expected if the response were only due to the equivalent amount of scintillator in the calorimeter. This result was confirmed also by the official Monte Carlo simulation of the KLOE experiment. To understand the underlying physical mechanisms which produce this difference, and to make a more systematic study of the calorimeter response, we planned a test beam to expose the calorimeter to a dedicated neutron beam and we developed a complete simulation of the detector geometry and response.

Apart from the possibility to develop compact, inexpensive, fast and highly efficient neutron counters, this work has also been motivated by the prospects of the search for deeply bound kaonic nuclei [6] and of the neutron electromagnetic form factor measurements in the time-like region [7]. These are two fundamental items for the DAΦNE upgrade under study at the Laboratori Nazionali di Frascati of INFN (LNF). In both cases the neutron detection efficiency is a key point for the measurements.

II. Measurement of the neutron detection efficiency at TSL

The KLOE calorimeter prototype used in this measurement is composed of $\sim$ 200 layers of 1 mm diameter blue scintillating fibers glued inside grooved lead layers of 0.5 mm thickness. The final structure has a fiber:lead:glue volume ratio of 48:42:10 resulting in a density of $\sim$ 5 g/cm^3. The total external dimensions are $13 \times 24 \times 65$ cm^3 where the second value is the calorimeter depth and the third one is the fiber length. The calorimeter is readout at both fiber ends in order to reconstruct this coordinate by time difference.

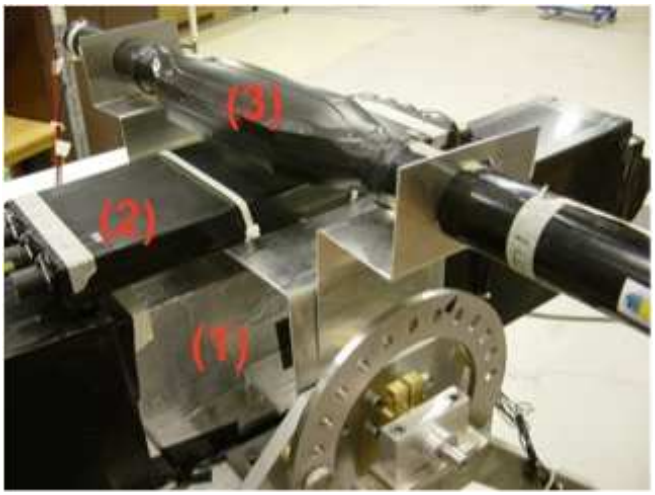

Fig. 1. Experimental setup used during test beam. (1) Calorimeter prototype, (2) beam position monitor and (3) NE110 reference counter.

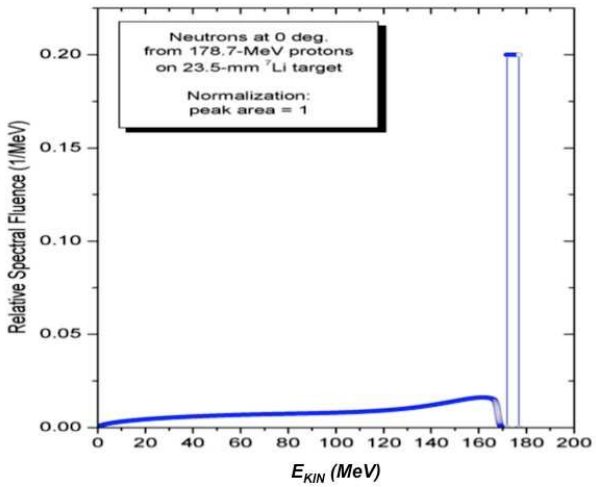

Fig. 2. Neutrons energy spectrum at the TSL facility.

The readout is organized in four planes along the calorimeter depth for the first 16.8 cm. Each plane is then divided in 3 columns along the horizontal coordinate originating cells of 4.2×4.2 cm^2. Larger readout elements are used in the rear part of the calorimeter. The small elements are coupled to 1-1/8 inch diameter standard bialkali photomultipliers, PM, through light guides.

When running with neutron beam, the calorimeter was positioned with fibers running vertically, the lower (upper) end is called side A (B). Each PM signal has been split in three replicas. The first two signals allow measurements of charge and time while the third one is used to summing up the PM charges of the first four planes of each side. The discriminated signals obtained, SA and SB, are combined in overlap coincidence, $SA \cdot SB$, to trigger on the calorimeter.

A reference counter for the efficiency measurement was built with a 5 cm thick bulk of NE110 organic scintillator, of transversal dimensions 10×20 cm^2, by coupling it at the two ends to two EMI9814 PM's.

A "beam position monitor" is also used. This detector was made by an array of seven scintillating counters 1 cm thick to check the beam shape during run.

The experimental setup is shown in Fig. 1, where we have the calorimeter prototype, the reference counter and the beam position monitor used to detect beam dimensions.

When running with the beam, the scintillator was positioned with its longest dimension along the horizontal coordinate. To trigger on the scintillator, the PM signals, $S1$ and $S2$, were discriminated and an overlap coincidence, $S1 \cdot S2$, was formed. We ran our experiment at the "The Svedberg Laboratory" (TSL) high-energy neutron facility [8]. At this facility, protons from the Gustaf Werner cyclotron were directed on a ^{7}Li target generating a neutron beam which is then geometrically shaped by an iron collimator block with a 2 cm diameter cylindrical hole. The energy and angular distributions of neutrons are defined by the differential cross section of the ^{7}Li(p,n) reaction at forward angles [9]. The neutron energy spectrum is dominated by a peak at a few MeV below the primary proton energy, and a long tail down to thermal neutrons (see Fig. 2). In our settings, we performed two different test beams, using high energy neutrons (178.7 MeV) and low energy neutrons (21 and 46 MeV). The neutron beam time structure was in phase with the cyclotron RF which had a period, T_{RF}, of $\sim$ 45 ns. The beam was emerging from the collimator at 3 m distance from the target. In order to ensure full beam acceptance we ran at a distance of 5.1 m from the target and centered the beam in the middle of our detectors. Very low intensity neutron beams, from 1.5 kHz/cm^2 to 6 kHz/cm^2, have been required in order to minimize the probability of counting more than a neutron per event. The neutron rate has been measured with a ionization-chamber monitor (ICM), with an absolute accuracy estimated at the level of 10 %.

All discrimination and trigger signals were formed with NIM logic while the DAQ was based on VME standard. Data have been acquired with a simplified version of the KLOE data acquisition system, composed by 40+40 ADC and TDC channels and able to write on disk at a rate of 1.7 kHz. The effective ADC gate was 300 ns wide, while the TDC worked in common start mode with the start provided by the trigger and the stop given by the discriminated signals delayed of 150 ns by a monostable inside the board. The trigger signal was either $SA \cdot SB$ or $S1 \cdot S2$ after phase locking with the cyclotron RF replica. Typical runs consist of $\sim 0.5 - 1.5 \times 10^6$ events.

The detector efficiency to the overall neutron spectrum, ϵ_D, has been determined taking the ratio of the counted detector rate, R_D, with the rate of the neutron beam estimated by the ICM, R_n. For a given trigger threshold, assuming full beam acceptance and no background, R_D is the ratio between the acquired rate, R_{DAQ}, and the fraction of DAQ live time, F_{live}. The incoming neutron rate, R_n, is instead given by:

$$R_n(\text{kHz}) = 9.09\ \pi \cdot R_{ICM} \cdot F_{peak}$$

where R_{ICM} is the ICM rate in Hz counted in each run and F_{peak} is the fraction of neutrons at peak energy.

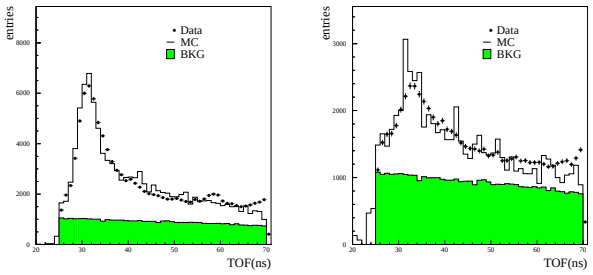

Fig. 3. Data-Monte Carlo comparison of time of flight in the central calorimeter cell for the first calorimeter plane with 174 MeV neutrons. Dots are data, histograms are the simulation (solid) and background (green) contributions. (left) central cell, (right) outer cell.

III. Calibration and measured efficiencies

For the scintillator, the horizontal scale has been calibrated fitting the energy spectra obtained with a reference β source. For the calorimeter, each cell has been calibrated using minimum ionizing particles and then applying the energy scale determined with electron and photon beams [10] in the same prototype.

The effective trigger thresholds cut-off have been evaluated from the data looking at the charge integrated by all the cells of the calorimeter at different thresholds. The ratio of these distributions normalized to the tail integrals has been fit with a Fermi-Dirac functions to extract the effective threshold value.

A clustering procedure is used to reconstruct the timing in the whole calorimeter and derive the kinetic energy of the primary neutron from time of flight, TOF. A first data-Monte Carlo comparison of TOF has been made at cell level. In the cells of the central column more than 90 % of the beam is contained. Data reconstructed clusters, with a single fired cell, show a ratio lateral/central fired cells higher then what expected from the simulation. Moreover, lateral cells show a flatter time distribution compared with Monte Carlo. We interpreted this effect as a presence of background due to low energy neutrons that form an halo around the central beam core. An overall good agreement is observed when taking into account also the shape of the halo contribution; this is obtained from data looking at the TOF distribution of the outer cells of the calorimeter where the background contamination is evident. We have estimated, for the run at 174 MeV, that halo events contribute to $\sim 30\%$ of the total number of events. In Fig. 3, we show the TOF distribution for the central and the outer cells of the first calorimeter plane.

Concerning low energy run, we are still completing the TOF study to evaluate the correct halo fraction. As a preliminary evaluation, we rely on halo measurement carried out by TSL beam experts. They performed a scan of the area near the collimator using a fission monitor counter. This measurement has been confirmed by our background counters. By integrating over the whole calorimeter plane, we estimate a fraction of halo contamination: $F_h = (20 \pm 10)\%$.

The measured efficiencies for the scintillator and for the calorimeter are shown in Fig. 4, and Figs.5 and 6, as a function of the trigger threshold in MeV, after correcting for the halo

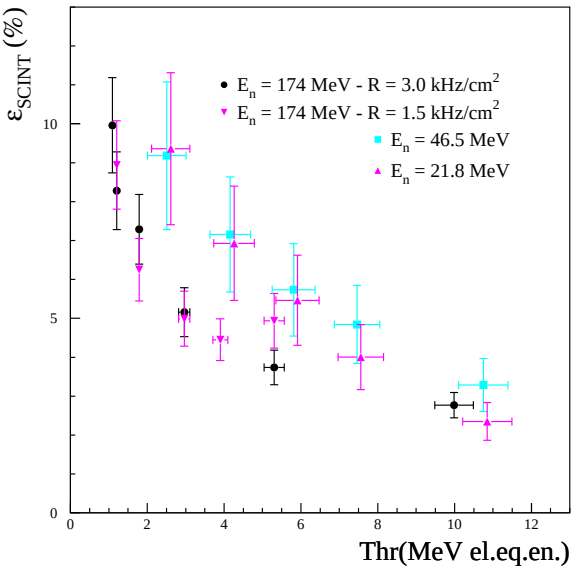

Fig. 4. Dependence of ϵ_{scint} on the applied trigger threshold. The horizontal scale is in MeV of electron equivalent energy. The systematics is 10 % on both horizontal and vertical scale. A comparison with available measurements in literature [1] is also shown.

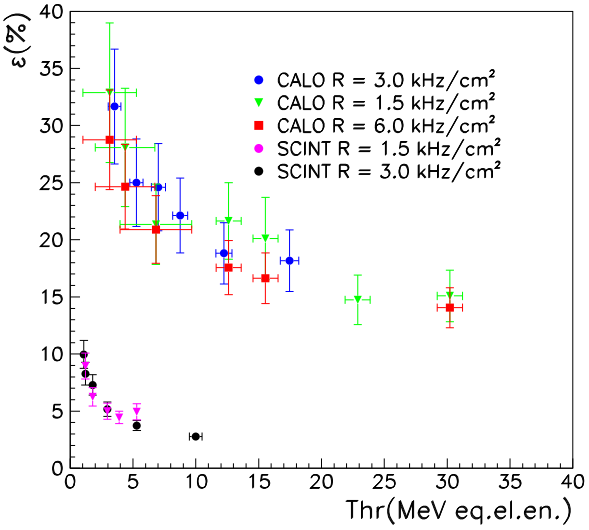

Fig. 5. Dependence of ϵ_{calo} on the trigger threshold (run at E_n 174 MeV). The horizontal scale is in MeV set for electron response.

fraction. In Figs.5 and 6, the calorimeter efficiency is also compared with the expected result obtained considering the scintillator equivalent thickness.

These results show that at the lowest trigger threshold the neutron detection efficiency of the calorimeter ranges from 28 % to 33 %, depending on the beam intensity. For comparison, the efficiency of the 5 cm thick NE110 scintillator ranges from 4 % to 10 %, for values of the trigger threshold below 5 MeV of electron equivalent energy, in good agreement with the available measurements in literature. This indicates

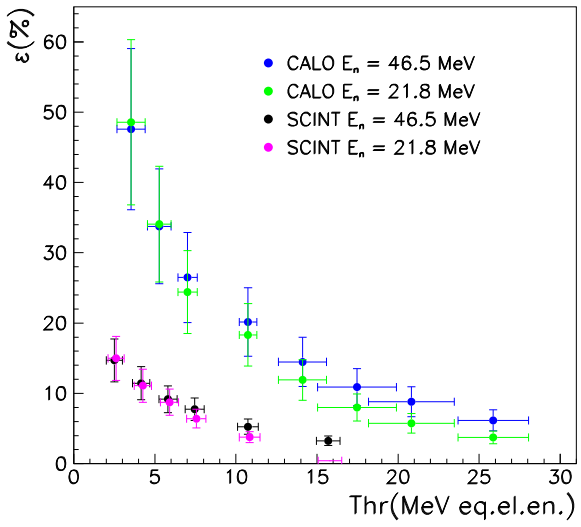

Fig. 6. Dependence of ϵ_{calo} on the trigger threshold (run at E$_n$ ∼21 MeV and E$_n$ ∼46 MeV). The horizontal scale is in MeV set for electron response.

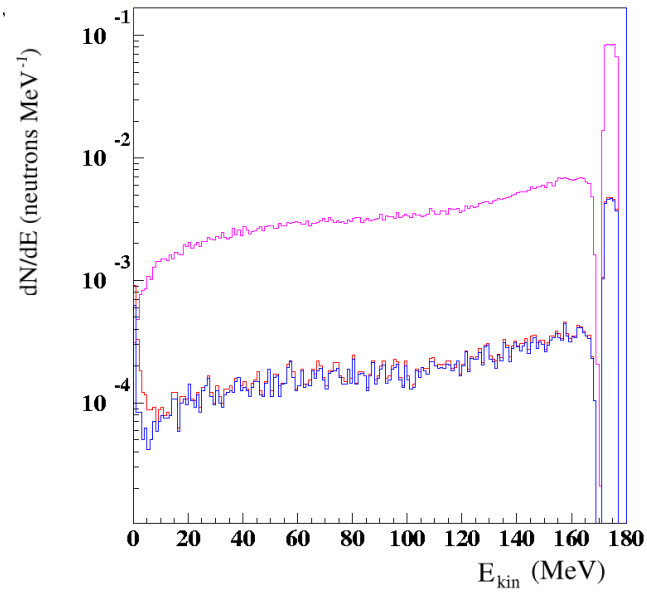

Fig. 7. Neutron energy spectra as computed with the FLUKA simulation. From the top: at the source, at the collimator exit and on the calorimeter entrance.

that the measured calorimeter efficiency is sizeably enhanced with respect to the expected 8−10% based on the amount of scintillator only.

IV. Monte Carlo simulation and comparison with data

The Monte Carlo code FLUKA [11], [12] has been used for a detailed simulation of the calorimeter structure. The TSL experimental beam-line, from the neutron source to the collimated beam, has been also simulated, in order to have a reliable characterization of the neutron beam impinging on the detector (see Fig. 7). Using the tool "LATTICE" the whole calorimeter module has been designed. All the compounds have been carefully simulated: for the fibers, an average density between cladding and core has been used, for the glue we have taken into account the right fraction of epoxy resin and hardener. FLUKA computes the energy deposits in the scintillating fibers, taking into account the signal saturation due to the Birks law. For each energy deposit, the average number of photoelectrons is estimated and then attenuated to the calorimeter ends with the proper attenuation length. The photoelectron statistics and the generation of the discriminated signal are also simulated, while the trigger effect has not yet been included.

The primary reason for the observed efficiency enhancement appears to be the huge inelastic production of neutrons on the lead planes. For neutrons in the high energy peak (175 MeV), the probability to have an inelastic interaction is 31.4 % on the lead, compared to 7.0 % on the fiber and 2.2 % on the glue. The secondary particles generated in such inelastic interactions are on average 5.4 per event, counting only the secondary neutrons above 19.6 MeV. Among the produced secondaries, 62 % are neutrons, 27 % photons, 7 % protons while the remaining 4 % are nuclear fragments. Typical inelastic reactions on lead are:

- n Pb $\rightarrow$ xn + $y\gamma$ + Pb,
- n Pb $\rightarrow$ xn + $y\gamma$ + p + residual nucleus,
- n Pb $\rightarrow$ xn + $y\gamma$ + 2p + residual nucleus.

Low-energy neutrons (below 19.6 MeV) are transported in FLUKA with a multi-group algorithm, that uses a neutron cross-section library derived from the most recently evaluated data. These secondary neutrons give also a sizeable contribution to the response: due to the larger inelastic cross section the neutron shower-like effect increases and originates on average about 100 secondaries per event, out of which ∼ 5 protons and ∼ 1 photon directly contribute in generating a visible response.

The high sampling frequency of the calorimeter appears to be a crucial point in the efficiency enhancement. First of all, the protons and the electromagnetic energy produced on lead in the inelastic processes can be detected by the nearby fibers down to very low energies. Moreover, secondary neutrons are produced on following lead planes with decreasing energies, thus having larger probabilities to produce ionizing particles on the nearby fibers. The isotropic distributions, which characterize the inelastic processes, also play a role: the back scattered neutrons contribute to increase the collision density in the first calorimeter planes, so containing the neutron shower depth.

A good agreement between data and simulation is observed when taking into account also the halo contribution as shown in Fig. 3 for the TOF and in Fig. 8 for the collected charge.

In Fig. 9 we show the dependence of ϵ_{calo} as a function of the trigger threshold compared to the FLUKA simulation after correcting R_{DAQ} for the halo contribution estimated with the TOF. The comparison is done for the run at 174 MeV. A pretty good data/simulation agreement is observed. Comparison between data and Monte Carlo for the low energy run is in progress.

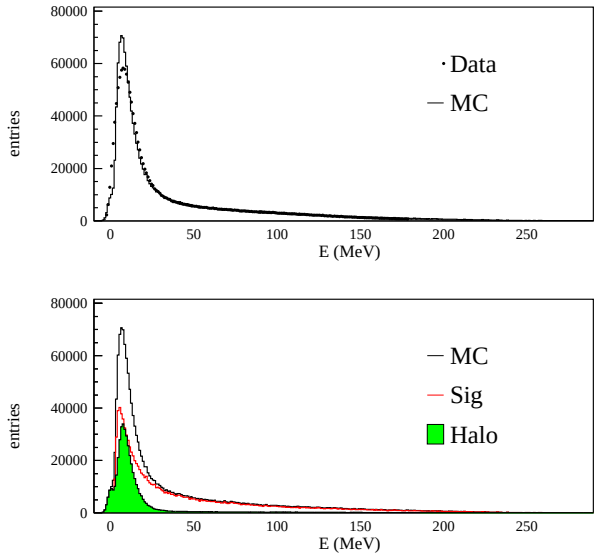

Fig. 8. Comparison between data and Monte Carlo for the collected charge. Halo contribution has been included in the simulation (bottom plot).

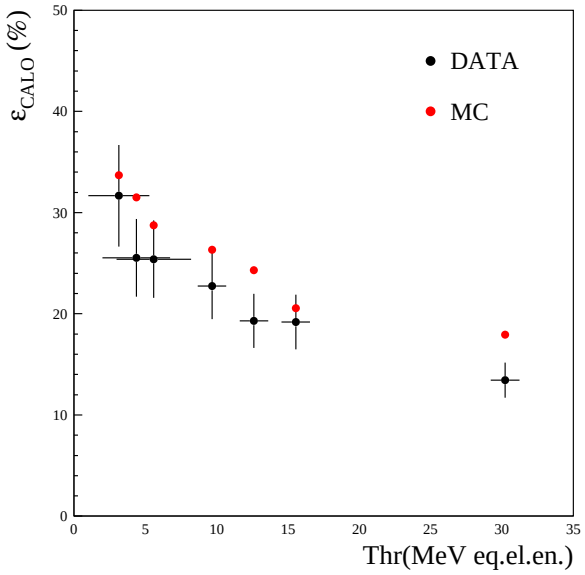

Fig. 9. ϵ_{calo} comparison between data (bullet) and simulation (open circle) as function of the applied trigger threshold for the run at 174 MeV.

V. Conclusion and prospects

Using an high sampling Pb-scintillating fibers calorimeter, the first measurement of the detection efficiency for neutrons between 20 and 180 MeV has been performed at the "The Svedberg Laboratory" of Uppsala. The calorimeter efficiency, integrated over the whole neutron energy spectrum, ranges between 32-50% at the lowest trigger threshold. This result is between three and four times larger than what expected considering the equivalent scintillator thickness of the prototype. Cross-check measurement of the neutron efficiency has been done using a NE110 scintillator. This result agrees with previous published results.

Monte Carlo simulation shows that the origin of such enhancement is related both to the shower-like effect due to the inelastic processes in the calorimeter structure and to the high sampling fraction of the detector. Preliminary comparison between data and Monte Carlo is satisfactory. Full simulation of the calorimeter, of the beam line and of the experimental hall (together with local shielding) is in progress.

We performed a last data taking campaign in 2008 fall at TSL. We used some new detectors to explain the physical effects observed. To better describe the beam halo, we built a new beam position monitor with $(1 \times 1)\ cm^2$ granularity read out using multianodes photomultipliers. We prepared a high granularity calorimeter prototype to study the processes inside the modules with best resolution. For this last test beam, we also built a small calorimeter with the same structure of the used prototype but with different sampling fraction. In particular, this last detector has more lead in its composition, and this is important to better study the efficiency enhancement that is predicted by Monte Carlo has due to the secondary interactions of neutron with the high Z material. The analysis of the acquired data is in progress.

Acknowledgment

We thank M. Arpaia, G. Bisogni, A. Cassarà, A. Di Virgilio, U. Martini, A. Olivieri and all the mechanical LNF division for the help in the construction of the NE110 reference counter and the overall mechanical supports. We also acknowledge A. Balla for the help in the setting of the electronic chain. We cannot forget to thank P. Caponera and M. Rossi, which have boldly transported all materials in the long trip from LNF to TSL. Moreover we want to warmly acknowledge all the TSL staff for the help during the data taking. This work was partially supported by "Transnational access to Research Infrastructure" TARI - The Svedberg Laboratory, HadronPhysics I3, Contract No. RII3-CT-2004-506078.

References

[1] A. Del Guerra, NIM **135** (1976) 319-330.
[2] C.Birattari et al., NIM **A 297** (1990), 250-257.
[3] C.Birattari et al., NIM **A 338** (1994), 534-543.
[4] The KLOE collaboration, NIM **A 482** (2002) 364-386.
[5] B. Sciascia, www.lnf.infn.it/kloe/klone/memoneueff.pdf
[6] LOI_MARCH_AMADEUS.pdf in http://www.lnf.infn.it/lnfadmin/direzione/roadmap/.
[7] loi_06.pdf in http://www.lnf.infn.it/conference/nucleon05/FF.
[8] A.V. Prokofiev et al., PoS (FNDA2006) 016 (2006).
[9] A.V. Prokofiev et al., Journal of Nuclear Science and Technology, Supplement 2 (2002), 112-115.
[10] A. Antonelli et al., NIM **A 354** (1995), 352-363.
[11] A. Fassò et al., CERN 2005-10 (2005), INFN/TC_05/11, SLAC-R-773.
[12] A.Fassò et al., eConf C0303241 (2003), arXiv:hep-ph/0306267.